Proceedings of the 2003 IEEE International Frequency Control Symposium and PDA Exhibition
Jointly with the 17th European Frequency and Time Forum

STRESS-INDUCED FREQUENCY SHIFTS IN LANGASITE THICKNESS-MODE RESONATORS

J. A. Kosinski[1], R. A. Pastore[1], Jr., X. Yang[2], J. Yang[2], and J. A. Turner[2]
[1]U.S. Army CECOM, Fort Monmouth, NJ, U.S.A.
[2]Department of Engineering Mechanics, University of Nebraska, Lincoln, NE, U.S.A.

Abstract - **In this paper, we report on our study of stress-induced effects on thickness vibrations of a langasite plate. The plate is assumed to be doubly-rotated, specified by angles ϕ and θ. The stresses are assumed to be uniform and planar. The first-order perturbation integral as developed by Tiersten for frequency shifts in resonators is used. The dependence of frequency shifts on ϕ and θ is calculated and examined, and loci of stress-compensation are determined. The analysis makes use of the third-order material constants that are available for langasite but not for its isomorphs.**
Keywords **– Langasite, stress-induced effects**

I. INTRODUCTION

The resonant frequencies of a piezoelectric resonator change when subjected to mechanical stresses. A variety of stress-induced effects in quartz resonators have been studied thoroughly, leading to, for example, the stress-compensated SC-cut quartz resonator [1,2]. Force-frequency and related effects in resonators made from langasite ($La_3Ga_5SiO_{14}$ or LGS), and its isomorphs are of current interest to the piezoelectric devices community [3-6]. Stress-induced frequency shifts in these resonators can be calculated using the perturbation approach detailed in [7]. A complete description of the linear effects of stresses on the resonant frequencies requires the knowledge of the third-order material constants. For LGS, these material constants have become available recently [8-11], and have been used in calculations of frequency shifts in STW, SAW, and BAW resonators [3-5]. Here we study stress-induced effects on the thickness vibration frequencies of an LGS plate.

The first-order perturbation approach for frequency shifts in resonators from [7] is summarized in Sec. II. The assumed uniform and planar stresses are given in Sec. III. Solutions for thickness vibration frequencies and modes when the stresses are not present are described in Sec. IV. Expressions for frequency shifts of pure thickness modes induced by planar stresses are obtained in Sec. V. Force sensitivity coefficients due to a pair of diametral forces and electrode film stress are discussed in Sec. VI. Numerical calculations of various force sensitivity coefficients for langasite resonators are presented in Sec. VII, along with comparisons to quartz resonators. Finally, some conclusions are drawn in Sec. VIII.

II. PERTURBATION INTEGRAL FOR FREQUENCY SHIFTS IN RESONATORS

The first-order description of frequency shifts in piezoelectric resonators due to initial or biasing mechanical fields can be calculated via a first-order perturbation analysis [7], whose essence is captured in the "perturbation integral"

$$\Delta\omega = \omega - \omega_0 = \frac{1}{2\omega_0}\frac{\int_V \hat{c}_{L\gamma M\alpha} u_{\gamma,L} u_{\alpha,M}\, dV}{\int_V \rho_0 u_\alpha u_\alpha dV} \tag{1}$$

where ω is the perturbed resonant frequency when the biasing fields are present, and ω_0, u_α, V, and ρ_0 respectively are the unperturbed resonant frequency, the corresponding mode, the volume of the crystal resonator, and the mass density in the reference configuration when there are no biasing fields. The effective elastic constants $\hat{c}_{L\gamma M\alpha}$ of the crystal under biasing fields (considering here purely elastic nonlinearities) are given by

$$\begin{aligned}\hat{c}_{K\alpha L\gamma} = {} & c_{K\alpha LN} w_{\gamma,N} + c_{KML\gamma} w_{\alpha,M} \\ & + c_{K\alpha L\gamma AB} w_{A,B} + c_{KLAB} w_{A,B}\delta_{\alpha\gamma}\end{aligned} \tag{2}$$

where **w** is the biasing displacement vector and $\delta_{\alpha\gamma}$ the Kronecker delta. c_{ABCD} and c_{ABCDEF} are the second- and third-order fundamental elastic constants. The plate is assumed to be doubly-rotated (Fig. 1), specified by angles ϕ and θ.

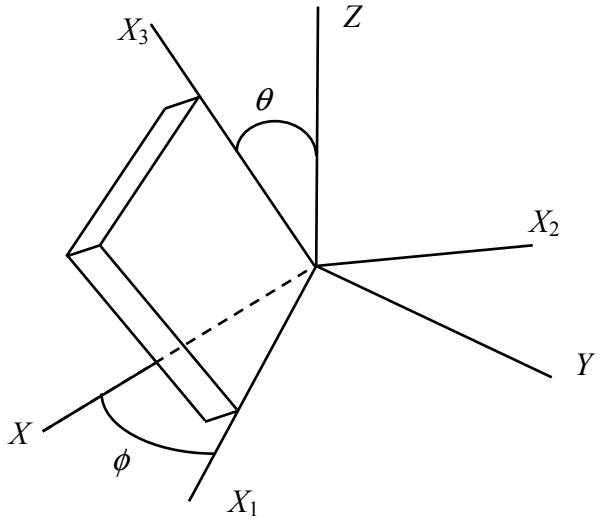

Fig. 1 Definitions of and second rotation angles ϕ and θ for a doubly-rotated crystal plate specified as (YXwl)φ,θ.

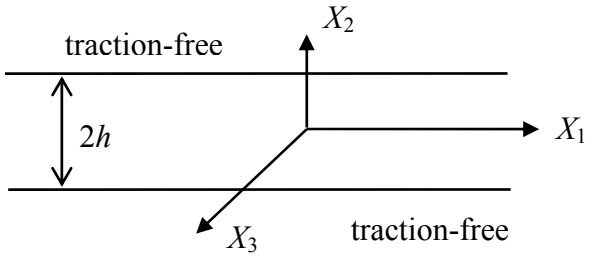

Fig. 2 A doubly-rotated crystal plate in the reference coordinate system.

III. Biasing Stresses

Consider a doubly-rotated langasite plate whose reference configuration without biasing fields is shown in Fig. 2. The biasing deformations are assumed to be small and are governed by the linear theory of anisotropic elasticity. We consider biasing deformations caused by the following planar state of stress:

$$\begin{aligned} &T_2^0 = T_4^0 = T_6^0 = 0, \\ &T_1^0, \quad T_3^0, \quad \textit{and} \quad T_5^0 \quad \textit{are constants.} \end{aligned} \tag{3}$$

We note that the above state of stress satisfies the traction-free boundary conditions at the major surfaces of the plate, the equilibrium and the compatibility equations of elasticity and is therefore an exact stress solution to the theory of linear elasticity. The strain components corresponding to (3) can be calculated from

$$E_p^0 = s_{pq} T_q^0, \quad p,q = 1,2,\cdots,6, \tag{4}$$

where s_{pq} is the compliance matrix. It has been shown that the change resonant frequency due to a homogeneous, infinitesimal rigid biasing rotation vanishes. Therefore we select the homogeneous rigid rotation to vanish, and the biasing displacement gradients are given simply by [12]

$$w_{K,L} = E_{KL}^0. \tag{5}$$

IV. Unperturbed Thickness Modes

For time harmonic thickness vibrations independent of X_1 and X_3, the equations of motion for the plate in Fig. 2 assume the following form

$$\begin{aligned} &c_{66}u_{1,22} + c_{62}u_{2,22} + c_{64}u_{3,22} = -\rho_0\omega^2 u_1, \\ &c_{26}u_{1,22} + c_{22}u_{2,22} + c_{24}u_{3,22} = -\rho_0\omega^2 u_2, \\ &c_{46}u_{1,22} + c_{42}u_{2,22} + c_{44}u_{3,22} = -\rho_0\omega^2 u_3, \end{aligned} \tag{6}$$

where ω is the unperturbed frequency, or ω_0 in (1). We assume traction-free boundary conditions at the two major surfaces of the plate at $X_2 = \pm h$

$$\begin{aligned} &T_{21} = c_{66}u_{1,2} + c_{62}u_{2,2} + c_{64}u_{3,2} = 0, \\ &T_{22} = c_{26}u_{1,2} + c_{22}u_{2,2} + c_{24}u_{3,2} = 0, \\ &T_{23} = c_{46}u_{1,2} + c_{42}u_{2,2} + c_{44}u_{3,2} = 0. \end{aligned} \tag{7}$$

We consider the following anti-symmetric thickness modes that are excitable electrically by a thickness electric field

$$u_j = A_j \sin kX_2, \tag{8}$$

where the A_j are undetermined constants. Substitution of (8) into (6) results in a system of homogeneous linear algebraic equations for the A_j

$$\begin{bmatrix} \rho_0\omega^2 - c_{66}k^2 & -c_{62}k^2 & -c_{64}k^2 \\ -c_{62}k^2 & \rho_0\omega^2 - c_{22}k^2 & -c_{42}k^2 \\ -c_{64}k^2 & -c_{42}k^2 & \rho_0\omega^2 - c_{44}k^2 \end{bmatrix} \begin{bmatrix} A_1 \\ A_2 \\ A_3 \end{bmatrix} = 0 \tag{9}$$

For nontrivial solutions, the determinant of the coefficient matrix of (9) must vanish, which leads to a polynomial equation of degree three for k^2. The equation has three branches of solutions for the dispersion relation $k^{(i)}(\omega)$, or equivalently three solutions of wave speed $\omega / k^{(i)}$. The corresponding eigenvectors $A_j^{(i)}$ are normalized in such a way as to provide a set of unique $\beta_j^{(i)}$, and the general anti-symmetric solution to (6) becomes

$$u_j = \sum_{i=1}^{3} B^{(i)} \beta_j^{(i)} \sin k^{(i)} X_2, \tag{10}$$

where the $B^{(i)}$ are undetermined constants. Substituting (10) into the boundary conditions in (7), we have

$$\begin{aligned} &T_{21} = \sum_{i=1}^{3} \gamma_1^{(i)} B^{(i)} k^{(i)} \cos k^{(i)} h = 0, \\ &T_{22} = \sum_{i=1}^{3} \gamma_2^{(i)} B^{(i)} k^{(i)} \cos k^{(i)} h = 0, \\ &T_{23} = \sum_{i=1}^{3} \gamma_3^{(i)} B^{(i)} k^{(i)} \cos k^{(i)} h = 0, \end{aligned} \tag{11}$$

where

$$\gamma_1^{(i)} = c_{66}\beta_1^{(i)} + c_{62}\beta_2^{(i)} + c_{64}\beta_3^{(i)},$$
$$\gamma_2^{(i)} = c_{26}\beta_1^{(i)} + c_{22}\beta_2^{(i)} + c_{24}\beta_3^{(i)}, \quad (12)$$
$$\gamma_3^{(i)} = c_{46}\beta_1^{(i)} + c_{42}\beta_2^{(i)} + c_{44}\beta_3^{(i)}.$$

Eq. (11) is a system of linear, homogeneous equations for the $B^{(i)}$. For nontrivial solutions, the determinant of the coefficient matrix of (11) has to vanish, which yields the frequency equation

$$\begin{vmatrix} \gamma_1^{(1)}k^{(1)}\cos k^{(1)}h & \gamma_1^{(2)}k^{(2)}\cos k^{(2)}h & \gamma_1^{(3)}k^{(3)}\cos k^{(3)}h \\ \gamma_2^{(1)}k^{(1)}\cos k^{(1)}h & \gamma_2^{(2)}k^{(2)}\cos k^{(2)}h & \gamma_2^{(3)}k^{(3)}\cos k^{(3)}h \\ \gamma_3^{(1)}k^{(1)}\cos k^{(1)}h & \gamma_3^{(2)}k^{(2)}\cos k^{(2)}h & \gamma_3^{(3)}k^{(3)}\cos k^{(3)}h \end{vmatrix} = 0 \quad (13)$$

that is equivalent to

$$\cos k^{(1)}h \cos k^{(2)}h \cos k^{(3)}h = 0\,. \quad (14)$$

The solutions for $k^{(i)}$ from (14) and the corresponding $B^{(i)}$ from (11) are

$$k^{(1)}(\omega) = \frac{n\pi}{2h}, \quad n = 1,3,5,\cdots, \quad B^{(1)} \neq 0, \quad B_2 = B_3 = 0,$$
$$k^{(2)}(\omega) = \frac{n\pi}{2h}, \quad n = 1,3,5,\cdots, \quad B^{(2)} \neq 0, \quad B_1 = B_3 = 0,$$
$$k^{(3)}(\omega) = \frac{n\pi}{2h}, \quad n = 1,3,5,\cdots, \quad B^{(3)} \neq 0, \quad B_1 = B_2 = 0. \quad (15)$$

The $k^{(i)}$ are functions of ω, thus ω can be determined from (15). The three sets of solutions in (15) represent respectively a series of thickness-stretch modes with a dominant u_2 and two series of thickness-shear modes with a dominant u_1 or u_3. These modes have the following expressions

$$u_j^{(i)} = B^{(i)}\beta_j^{(i)} \sin k^{(i)}X_2\,, \quad (16)$$

where i is not being summed.

Similarly to (8), a set of symmetric modes can be found for (6,7). In the absence of a thickness-direction asymmetry, the symmetric modes cannot be excited by a thickness electric field and therefore will not be considered here.

V. Frequency Shifts of Thickness Modes due to Planar Stresses

Real resonators are finite plates. For thickness-shear resonators the plates are usually very thin. We neglect edge effects and consider the above infinite plate thickness modes over the finite but symmetric two-dimensional region of $-a<X_1<a$ and $-c<X_3<c$. When the perturbation integral in (1) is applied to such a finite region with the above biasing fields and unperturbed modes, it turns out that the resulting frequency shift does not depend on a and c, as expected. For a particular mode of (16), the frequency shift is given by

$$\Delta\omega = \frac{k^2}{2\omega_0\rho_0\left(\beta_1^2+\beta_2^2+\beta_2^3\right)}\times \left[\hat{c}_{1212}\beta_1^2 + \hat{c}_{2222}\beta_2^2 + \hat{c}_{2323}\beta_3^2 + 2\hat{c}_{2212}\beta_1\beta_2 + 2c_{2312}\beta_1\beta_3 + 2\hat{c}_{2223}\beta_2\beta_3\right] \quad (17)$$

where k, ω, and β_j are all for a particular i of (16).

VI. Force Sensitivity Coefficients of Resonators

The effects of stresses on resonator frequencies are usually described in terms of the force sensitivity coefficients described below.

A Effect of a Pair of Diametral Forces

Consider a circular disk resonator of diameter D and thickness $2h$ under a pair of equal and opposite diametral forces F (Fig. 3). The x and z axes are along and perpendicular to the loading direction at an angle ψ from the X_1 axis. The exact stress distribution in an orthotropic crystal disk under a pair of diametral forces was given in [12]. For disks of general anisotropy the exact stress distribution is more complicated. In this analysis, as an approximation, the following stress [13] at the center of an isotropic disk under a pair of diametral forces is used throughout the resonator:

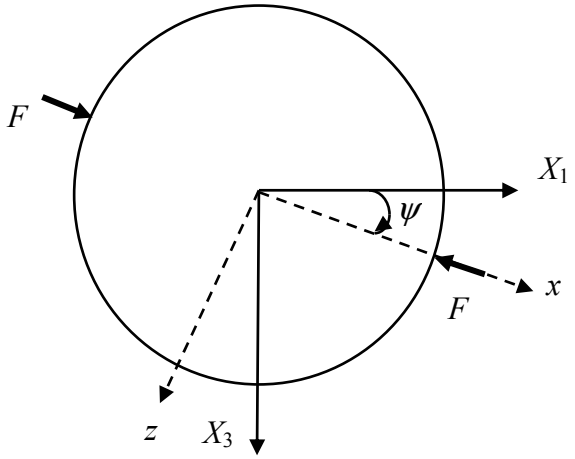

Fig. 3 A circular plate resonator under a pair of diametral forces.

$$T_{xx}^0 = -\frac{6}{\pi}\frac{F}{2hD}, \quad T_{zz}^0 = \frac{2}{\pi}\frac{F}{2hD}, \quad T_{xz}^0 = 0. \tag{18}$$

It has been found with quartz resonators, that using the simpler stresses (18) from an isotropic disk and then calculating the corresponding strains from anisotropic constitutive relations yields results close to those from experiments [14] and from a fully anisotropic stress analysis [12]. Therefore the same simplified approach is adopted here. The corresponding stress components in the X_1 and X_3 coordinate system are determined by tensor transformation as

$$\begin{aligned} T_1^0 &= -\frac{2}{\pi}\frac{F}{2hD}(1+2\cos 2\psi), \\ T_3^0 &= -\frac{2}{\pi}\frac{F}{2hD}(1-2\cos 2\psi), \\ T_5^0 &= -\frac{4}{\pi}\frac{F}{2hD}\sin 2\psi, \end{aligned} \tag{19}$$

and the corresponding strains are calculated from the anisotropic constitutive relations in (4).

The force sensitivity coefficient K_f is defined as [6,14,15]

$$\begin{aligned} K_f(\phi,\theta,\psi) &= \frac{\Delta f}{f_0}\frac{1}{F}\frac{nD}{f_0} = \frac{\Delta f}{f_0}\frac{2hD}{F}\frac{1}{f_0(2h/n)} \\ &= \frac{\Delta f}{f_0}\frac{(Thickness)(Diameter)}{(Force)(Acoustic\ velocity/2)}, \end{aligned} \tag{20}$$

where n is the harmonic overtone order of the thickness frequency, $f = \omega/2\pi$, $f_0 = \omega_0/2\pi$, and $\Delta f = f - f_0$. In our calculations, F = 9.81N and D = 14mm are used, and h is chosen such that the 5th overtone of the slow-shear mode (c-mode) is 10 MHz.

B. Effect of Electrode Film Stress

Electrode film stress is effectively a distribution of stress along the edge of the electrode on a resonator. The film stress sensitivity coefficient [16] is therefore the mean value of (20) [2,6]

$$< K_f(\phi,\theta) >= \frac{1}{\pi}\int_0^{\pi} K_f(\psi)d\psi\Big|_{\varphi,\theta}, \tag{21}$$

which is also referred to as the mean stress sensitivity coefficient. We note that $<K_f>$ is a function of the plate orientation angles ϕ and θ. A planar-stress-compensated orientation possesses a zero $<K_f>$ [12].

VII. Numerical Results and Discussions

For LGS, a consistent set of second-order material constants and the fourteen independent third-order elastic constants with respect to the crystallographic axes *XYZ* can be found from [8-11] as listed in Tables I and II. The corresponding values for quartz are included in the Tables for comparison.

TABLE I
LINEAR MATERIAL CONSTANTS OF LANGASITE AND QUARTZ

Constant	Langasite [8-11]	Quartz	Units
ρ	5743	2649	kg/m^3
ε_{11}^S	18.92	4.43	ε_0
ε_{33}^S	50.701	4.63	ε_0
e_{11}	-0.44	0.171	C/m^2
e_{14}	-0.08	-0.0406	C/m^2
c_{11}^E	188.75	86.74	GPa
c_{12}^E	104.75	6.98	GPa
c_{13}^E	95.89	11.91	GPa
c_{14}^E	-14.12	-17.91	GPa
c_{33}^E	261.4	107.2	GPa
c_{44}^E	53.5	57.94	GPa
c_{66}^E	42	39.88	GPa

TABLE II
NONLINEAR ELASTIC STIFFNESSES OF LANGASITE AND QUARTZ

Constant	Langasite [8-11]	Quartz	Units
c_{111}	-972	-210	GPa
c_{112}	7	-345	GPa
c_{113}	-116	12	GPa
c_{114}	-22	-163	GPa
c_{123}	9	-294	GPa
c_{124}	-28	-15	GPa
c_{133}	-721	-312	GPa
c_{134}	-41	2	GPa
c_{144}	-40	-134	GPa
c_{155}	-198	-200	GPa
c_{222}	-965	-332	GPa
c_{333}	-1834	-815	GPa
c_{344}	-389	-110	GPa
c_{444}	-202	-276	GPa

The other seventeen non-zero third-order elastic constants are given by the following relations [17]:

$$c_{122} = c_{111} + c_{112} - c_{222}, \qquad c_{156} = \frac{1}{2}(c_{114} + 3c_{124}),$$

$$c_{166} = \frac{1}{4}(-2c_{111} - c_{112} + 3c_{222}), \qquad c_{224} = -c_{114} - 2c_{124},$$

$$c_{256} = \frac{1}{2}(c_{114} - c_{124}), \qquad c_{266} = \frac{1}{4}(2c_{111} - c_{112} - c_{222}),$$

$$c_{366} = \frac{1}{2}(c_{113} - c_{123}), \qquad c_{456} = \frac{1}{2}(-c_{144} + c_{155}),$$

$$c_{223} = c_{113}, \qquad c_{233} = c_{133}, \qquad c_{234} = -c_{134},$$

$$c_{244} = c_{155}, \qquad c_{255} = c_{144}, \qquad c_{355} = c_{344},$$

$$c_{356} = c_{134}, \qquad c_{455} = -c_{444}, \qquad c_{466} = c_{124}. \tag{24}$$

From (22-24) and the tensor transformation rules the second- and third-order elastic constants for a doubly-rotated plate in the $X_1X_2X_3$ system can be obtained systematically.

For the langasite isomorphs langatate ($La_3Ga_{5.5}Ta_{0.5}O_{14}$ or LGT) and langanite ($La_3Ga_{5.5}Nb_{0.5}O_{14}$ or LGN), only the second-order elastic constants are available [18,19] and we are unable to perform similar calculations at this time.

A. Force-Frequency Effect in a Quartz Resonator

In order to verify the accuracy of our calculations, we have calculated $\langle K_f \rangle$ for the c-mode (slow shear) in a quartz resonator and have compared our results with those from [12] using the same isotropic stress distribution as (18). The results are shown in Table III. The agreement is very good overall, with a single exception.

TABLE III
MEAN FORCE SENSITIVITY COEFFICIENT $\langle K_f \rangle$ FOR C-MODE IN QUARTZ (10^{-15} m·s/N)

Orientation		Our results	Reference [12]
ϕ (Degree)	θ (Degree)		
0	32.25	10.72	10.7
10	34.08	7.40	7.4
15	34.08	4.80	4.81
19.1	34.08	2.24	2.25
30	34.08	-5.20	-4.82
21.9	34.08	0.36	0.37

B. Force-Frequency Effects in a Langasite Resonator

Fig. 4 shows the force sensitivity coefficients of the three thickness modes of a Y-cut LGS resonator. The curves are periodic in ψ with a period of 180°, as expected.

Following [13], we plot the mean force sensitivity coefficients for a Y-cut LGS resonator as functions of θ for a few values of ϕ in Figs. 5-8. These curves are periodic in θ with a period of 180°. When a curve intersects with the horizontal axis at a particular value of θ, the corresponding ϕ and θ represent a stress compensated cut. It can be seen that stress compensated cuts do exist for an LGS plate resonator. We note that in Fig. 5 there is a vertical line between the curves for the fast and slow shear modes at $\theta \cong$ -43°, which represents the cross-over of the two shear mode frequencies.

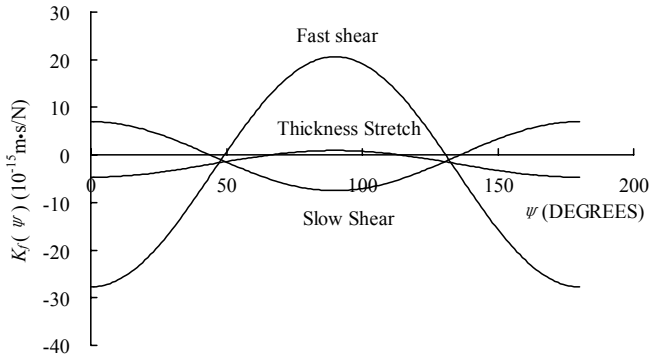

Fig. 4 Force-frequency coefficients of the simple thickness modes for a Y-cut langasite resonator.

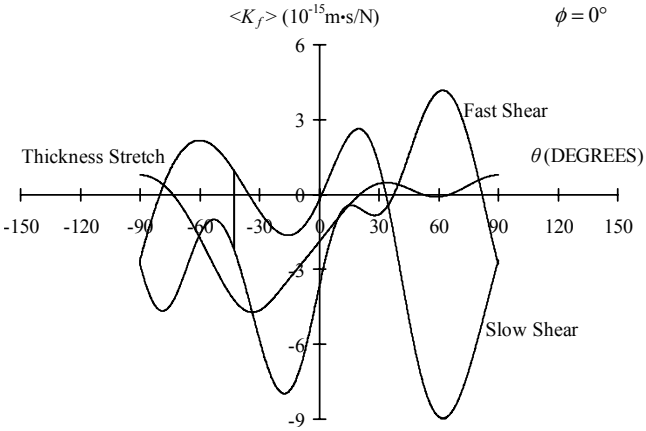

Fig. 5 Mean force sensitivity coefficients of a (YXwl)ϕ,θ langasite resonator for ϕ = 0° (also known as the family of rotated Y-cuts).

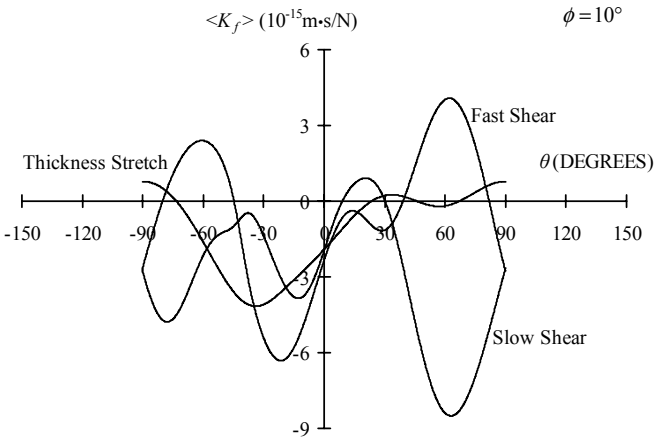

Fig. 6. Mean force sensitivity coefficients of a (YXwl)ϕ,θ langasite resonator for $\phi = 10^{o}$.

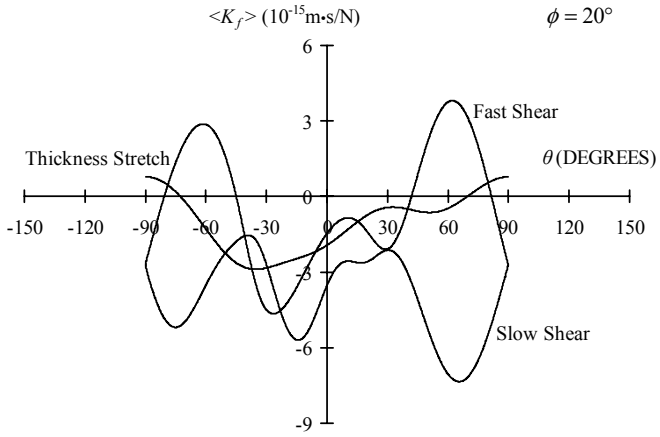

Fig. 7 Mean force sensitivity coefficients of a (YXwl)ϕ,θ langasite resonator for $\phi = 20^{o}$.

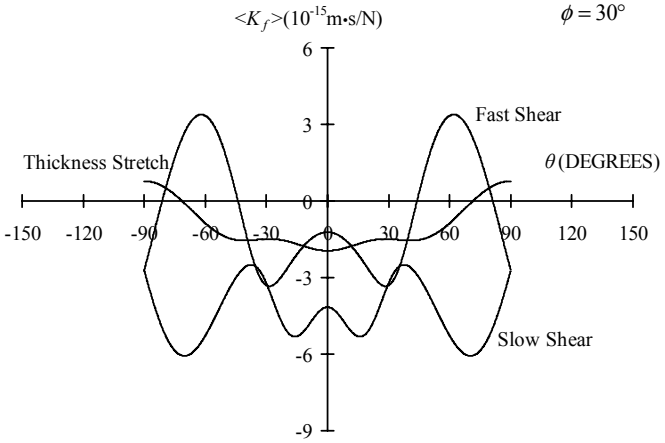

Fig. 8 Mean force sensitivity coefficients of a langasite resonator for $\phi = 30^{o}$.

It is of great practical interest to determine the loci of stress-compensation showing all cuts with a vanishing $<K_f>$ [13]. For the b-mode and c-mode these loci are given in Figs. 9 and 10. We observe that the locus for stress-compensation for the c-mode passes very near to the Y-cut.

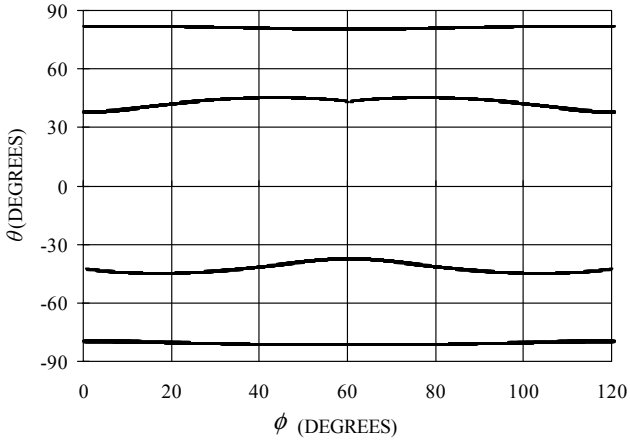

Fig. 9. Loci of stress compensation for the b-mode in an LGS resonator.

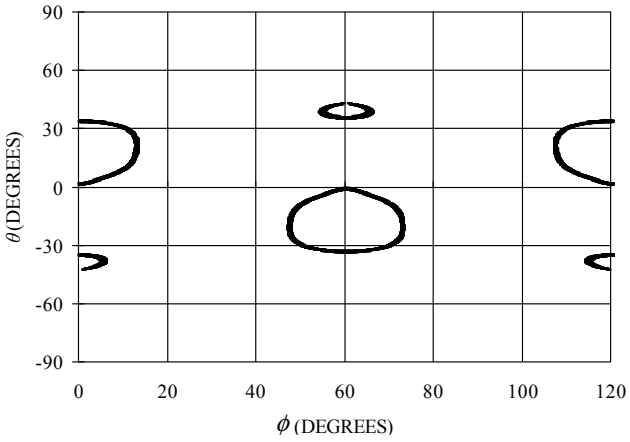

Fig. 10. Loci of stress compensation for the c-mode in an LGS resonator.

C. Comparison of Resonators of Different Materials

In Fig. 11 the force sensitivity coefficients of the c-modes in both AT-cut and SC-cut quartz resonators are compared with that of the LGS Y-cut c-mode resonator. It can be seen that the maximum force sensitivity values for the Y-cut LGS resonator are smaller than those of the two quartz resonators. The mean force sensitivity coefficients $<K_f>$ for these three resonators are compared in Table IV. It can be seen that the SC-cut quartz resonator has the smallest mean force sensitivity coefficient, however that of Y-cut LGS is only a factor of five larger, while that of AT-cut quartz is 275 times larger.

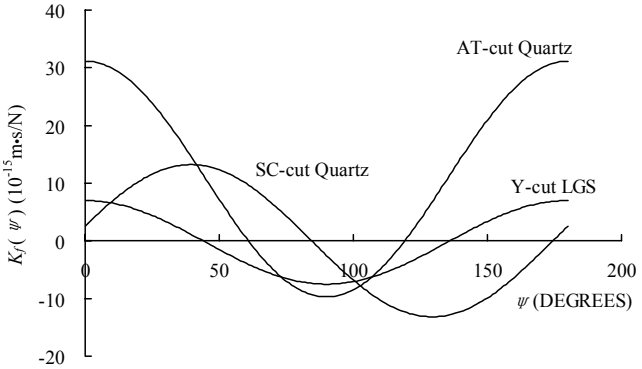

Fig. 11. Mean force sensitivity coefficients in resonators of different materials and cuts.

TABLE IV
COMPARISON OF MEAN FORCE SENSITIVITY COEFFICIENT $<K_f>$

Cut/Material	ϕ (Deg.)	θ (Deg.)	$<K_f>$ (10^{-15} m·s/N)
AT-cut/quartz	0	35.25	10.89
SC-cut/quartz	22.4	34.3	0.038
Y-cut/LGS	0	0	-0.22

VIII. CONCLUSIONS

The force sensitivity coefficients of a thickness-mode langasite plate resonator have been investigated using values of second- and third-order elastic constants from the prior literature. Loci of zero-mean planar force-sensitivity have been determined. Our calculations indicate the existence of stress-compensated cuts in langasite, and a high degree of stress-compensation for the LGS Y-cut c-mode resonator.

ACKNOWLEDGEMENT

This work was supported by the Army Research Office under DAAD19-01-1-0443.

REFERENCES

[1] E. P. EerNisse, "Quartz resonator frequency shifts arising from electrode stress," *Proc. 29th Frequency Control Symp.*, 1975, pp. 1-4.
[2] A. Ballato, E. P. EerNisse, and T. J. Lukaszek, "Experimental verification of stress compensation in the SC cut," *Proc. IEEE Ultrasonics Symp.*, 1978, pp. 144-147.
[3] J. A. Kosinski and R. A. Pastore, Jr., "Analysis of quartz and langasite STW device acceleration sensitivity," *Proc. IEEE Ultrasonics Symp.*, 2000, pp. 227-230.
[4] R. M. Taziev, "Stress, temperature and pressure behavior of SAW on langasite plates," *Proc. IEEE Int. Frequency Control Symp. and PDA Exhibition*, 2001, pp. 227-234.
[5] J. J. Boy, R. J. Besson, E. Bigler, R. Bourquin, and B. Dulmet, "Theoretical and experimental studies of the force-frequency effect in BAW LGS and LGT resonators," *Proc. IEEE Int. Frequency Control Symp. and PDA Exhibition*, 2001, pp. 223-226.
[6] Y. Kim and A. Ballato, "Force-frequency effects of Y-cut langanite and Y-cut langatate," *Proc. of the IEEE International Frequency Control Symp. and PDA Exhibition*, 2002, pp. 328-332.
[7] H. F. Tiersten, "Perturbation theory for linear electroelastic equations for small fields superposed on a bias," *J. Acoust. Soc. Am.*, vol. 64, pp. 832-837, 1978.
[8] K. S. Aleksandrov, B. P. Sorokin, P. P. Turchin, and D. A. Glushkov, "Non-linear Piezoelectricity in La3Ga5SiO14 Piezoelectric Single Crystal," Ferroelectrics Letters, vol. 14, 1992, pp. 115-125.
[9] B. P. Sorokin, P. P. Turchin, and D. A. Glushkov, "The Elastic Nonlinearity and Peculiarities of Bulk Acoustic Wave Propagation Under the Influence of Homogeneous Mechanical Stresses in La3Ga5SiO14 Single Crystals," Fizika Tverdogo Tela, vol. 36, no. 10, 1994, pp. 2907-2916.
[10] K. S. Aleksandrov, B. P. Sorokin, P. P. Turchin, S. I. Burkov, D. A. Glushkov, and A. A. Karpovich, "Effects of static electric field and of mechanical pressure on surface acoustic waves propagation in $La_3Ga_5SiO_{14}$ piezoelectric single crystals," *Proc. IEEE Ultrasonics Symp.*, 1995, pp. 409-412.
[11] B. P. Sorokin, P. P. Turchin, S. I. Burkov, D. A. Glushkov, and K. S. Alexandrov, "Influence of static electric field, mechanical pressure and temperature on the propagation of acoustic waves in $La_3Ga_5SiO_{14}$ piezoelectric single crystals," *Proc. IEEE Int. Frequency Control Symp.*, 1996, pp. 161-169.
[12] B. K. Sinha, "Stress-induced frequency shifts in thickness-mode resonators," *Proc. IEEE Ultrasonics Symp.*, 1980, pp. 813-818.
[13] B. K. Sinha, "Stress compensated orientations for thickness-shear quartz resonators," *Proc. 35th Ann. Freq. Control Symp.*, 1981, pp. 213-221.
[14] P. C. Y. Lee and K.-M. Wu, "In-plane accelerations and forces on frequency changes in doubly-rotated quartz plates," *J. Acoust. Soc. Am.*, vol. 75, pp. 1105-1117, 1984.
[15] J. M. Ratajski, "Force-frequency coefficient of singly rotated vibrating quartz crystals," *IBM J. Res. Dev.*, vol. 12, pp. 92-99, 1968.
[16] M. Mizan and A. Ballato, "The stress coefficient of frequency of quartz plate resonators," *Proc. 37th Ann. Freq. Control Symp.*, 1983, pp. 194-199.
[17] D. F. Nelson, *Electric*, *Optic*, *and Acoustic Interactions in Dielectrics*, New York: John Wiley & Sons, 1979.
[18] M. P. da Cunha, D. C. Malocha, E. L. Adler and K. J. Casey, "Surface and pseudo surface acoustic waves in langatate: predictions and measurements," *IEEE Trans. on Ultrasonics, Ferroelectrics, and Frequency Control*, vol. 49, pp. 1291-1299, 2002.
[19] Yu. V. Pisarevsky, P. A. Senyushenkov, B. V. Mill and N. A. Moiseeva, "Elastic, piezoelectric, dielectric properties of $La_3Ga_{5.5}Ta_{0.5}O_{14}$ single crystals," *Proc. IEEE Int. Frequency Control Symp.*, 1998, pp. 742-747.